Gold(III) Corroles for High Performance Organic Solar Cells

*Shiu-Lun Lai, Lin Wang, Chen Yang, Mei-Yee Chan, Xiangguo Guan, Chi-Chung Kwok, and Chi-Ming Che**

While the use of molecular materials having long-lived triplet excited state(s) for harvesting solar energy could be an effective approach to boost up the power conversion efficiency (PCE) of organic solar cells (OSCs), the performances of this kind of OSCs as reported in the literature are low (< 2.9% PCE attained for the vacuum-deposited OSCs). Herein, the realization of high performance OSCs by using gold(III) 5,10,15-triphenylcorrole (Au-C1), gold(III) 10-(*p*-trifluoromethylphenyl)-5,15-diphenylcorrole (Au-C2), and gold(III) 10-(pentafluorophenyl)-5,15-diphenyl-corrole (Au-C3), as electron-donors, is described. These gold(III) corroles display excited state lifetimes of ≥ 25 μs and low emission quantum yields of < 0.15%. With the complexes Au-C1, Au-C2, and Au-C3, vacuum-deposited OSCs, which give PCEs of 2.7%, 3.0%, and 1.8%, respectively, are fabricated. The PCE can be further boosted up to 4.0% after thermal treatment of the OSC devices. Meanwhile, a solution-processed OSC based on Au-C2 with a high PCE of 6.0% is fabricated. These PCE values are among the best reported for both types of vacuum-deposited and solution-processed OSCs fabricated with metal-organic complexes having long-lived excited states as electron-donor material. The underlying mechanism for the inferior performance of the reported OSCs is discussed.

1. Introduction

Due to its potential in cost-effective delivery of clean and renewable energy, organic solar cell (OSC) has continued to an area of immense interests.[1–34] Over the past decades, there has been significant progress in boosting the power conversion efficiency (PCE) of OSCs through the development of new smart functional materials, novel device configurations and fabrication techniques,[1–9] all of these are essential to the realization of the commercial practical application of OSCs technology. The highest PCEs of the current state-of-the-art electron donor–acceptor (D–A) single-junction OSCs based on small molecules, such as 2,4-*bis*[4-(*N*,*N*-diisobutylamino)-2,6-dihydroxyphenyl] squaraine (DIBSQ)-fullerene (C_{70}), and conjugated polymers, such as thieno[3,4-*b*]thiophene/benzodithiophene (PTB7)-[6,6]-phenyl-C_{71} butyric acid methyl ester ($PC_{71}BM$), have reached 6.1%[1] and 9.2%,[2] respectively. Recently, a record-high PCE beyond 10%[3,4] has been achieved using sophisticated tandem device architecture involving two D–A sub-cells in series connection to enhance the absorption of solar light. In OSCs, tightly bound excitons (i.e., hole-electron pairs) are generated within the photoactive materials upon photo-excitation. These excitons will migrate towards D–A interface and dissociate into free charge carriers, generating photocurrent. At the same time, some of them may undergo radiative and non-radiative decays in the course of exciton migration.[5] As the photo-generated singlet excitons have short lifetimes (only ~10^{-9} s) and tend to decay much rapidly, the diffusion length is short (L_D ≈ 1–10 nm, by inference, which is much shorter than absorption depth ≈100 nm required for light-absorption), leading to inferior photovoltaic (PV) performance. The use of metal-organic complexes[6,7,14–34] having long-lived triplet exciton states and long L_D may provide a solution to overcome this "exciton bottleneck". Indeed, some OSCs using organometallic complexes as triplet photoactive materials have been reported.[6,7,14–24,26,28–34] These organometallic complexes are predominately the ones containing cyclometalated ligand(s) and have been widely studied in phosphorescent organic light-emitting devices (PHOLEDs) because of their inherently long triplet excited state lifetimes (τ_t) as well as high luminescence quantum yields (Φ_{PL}).[35–38] It is envisaged that the presence of heavy metal atom would enable strong spin–orbit coupling that facilitates intersystem crossing (ISC) from singlet to triplet excited states. The long lifetimes of triplet excitons can significantly reduce exciton recombination and this is desirable for improving PCE values of OSCs. In addition, due to the strong mixing between triplet metal-to-ligand charge-transfer (MLCT) and singlet ligand-centered $\pi\rightarrow\pi^*$ excited states, these organometallic complexes usually display broad absorptions in the entire visible spectral region extending up to 800 nm.[39,40] The broad absorption is particularly beneficial to the improvement of OSC performance.

While the use of metal-organic/organometallic complexes offers a potential in the design of highly efficient OSCs, the performance of such OSCs as reported nowadays are much lagging behind from those fabricated using pure (or metal-free) molecular compounds or conjugated polymers. Particularly, the PCEs reported so far are less than 2.9%

Dr. S.-L. Lai, L. Wang, C. Yang, Dr. M.-Y. Chan, Dr. X. Guan, Dr. C.-C. Kwok, Prof. C.-M. Che
State Key Laboratory of Synthetic Chemistry
HKU-CAS Joint Laboratory on New Materials and Department of Chemistry
The University of Hong Kong
Pokfulam Road, Hong Kong
E-mail: cmche@hku.hk

DOI: 10.1002/adfm.201400082

for vacuum-deposited[6,14–24] or 5.0% for solution-processed devices.[7,24–34] Herein, we report a panel of gold(III) corroles (**Au-C**s), namely gold(III) 5,10,15-triphenylcorrole (**Au-C1**), gold(III) 10-(*p*-trifluoromethylphenyl)-5,15-diphenylcorrole (**Au-C2**), and gold(III) 10-(pentafluorophenyl)-5,15-diphenylcorrole (**Au-C3**), used as electron-donor in OSCs. These **Au-C** complexes have long τ_t of ≥ 25 μs. By blending the **Au-C** complexes with electron-acceptor C_{70}, the vacuum-deposited OSCs gave short-circuit current density (J_{SC}) of 8.97, 9.21, and 6.67 mA cm^{-2}, open-circuit voltage (V_{OC}) of 0.77, 0.82, and 0.88 V, and fill factors (FF) of 0.39, 0.40, and 0.30 (corresponding to the PCEs of 2.7%, 3.0%, and 1.8%) respectively when operated under illumination using a standard AM1.5G (AM: Air Mass; G: Global) simulated sunlight. After thermal treatment of these **Au-C**-OSCs, the PCE could be further boosted up to 4.0%. In addition, solution-processed OSC based on **Au-C2** with PCE of 6.0% has been achieved. These PCE values are among the best reported for both vacuum-deposited and solution-processed OSCs using metal-organic complexes as electron-donor. It is suggested that the Φ_{PL} of metal-organic complex plays an important role affecting the PCE of the as fabricated OSC and can be used to rationalize the inferior performance of the literature reported OSCs based on strongly luminescent metal-organic complexes.

2. Results and Discussion

2.1. Synthesis and Characterization of Au-Cs

The **Au-C1**, **Au-C2**, and **Au-C3** complexes were synthesized according to literature procedures.[41–44] The synthesis of **Au-C**s was reported by Thomas et al.[43] and Rabinovich et al. in 2011.[44] In this work, one of the phenyl rings of corrole ligand was functionalized with electron-withdrawing group in order to tune the absorption energy. The molecular structures and synthetic routes of **Au-C**s are depicted in **Scheme 1**. The **Au-C** complexes were purified by chromatography on silica gel column and were characterized by ^{1}H NMR spectroscopy (their ^{1}H NMR spectra are shown in Figure S1–S3 in Supporting Information (ESI)). They have a good solubility in common organic solvents, are stable toward air, and have high decomposition temperature of 355–371 °C (T_d corresponds to 5% weight loss in thermogravimetric analysis (TGA) measurement).

Figure 1a shows the absorption spectra of **Au-C1**, **Au-C2**, and **Au-C3** in degassed dichloromethane (DCM) at 298 K. They exhibit broad absorption bands at wavelength from 250–600 nm with strong Soret bands at around 420 nm (molar absorption coefficient $\varepsilon \approx 12.1–18.1 \times 10^4$ dm^3 mol^{-1} cm^{-1}). The Soret bands are attributed to $\pi \rightarrow \pi^*$ transitions of the corrole ligand. The absorption onset for **Au-C1**, **Au-C2**, and **Au-C3** are at around 591, 589, and 583 nm, respectively, corresponding to the optical band-gap (E_{opt}) of 2.10, 2.11, and 2.13 eV, respectively. The higher energy absorption bands with peak maxima at 281–287 nm and $\varepsilon \approx 1.7–2.3 \times 10^4$ dm^3 mol^{-1} cm^{-1} are attributed to ligand-to-ligand $\pi \rightarrow \pi^*$ charge transfer (LLCT) transitions of the corrole ligand. The lower energy absorption bands with peak maxima at 556–574 nm with $\varepsilon \approx 2.1–2.8 \times 10^4$ dm^3 mol^{-1} cm^{-1} are due to mixed ligand-to-metal charge-transfer (LMCT) and ligand-centered $\pi \rightarrow \pi^*$ transitions. The absorption peak maxima of **Au-C3** at 556 and 566 nm are blue-shifted by about 5 nm from those of **Au-C1**; a similar slight blue-shift of absorption peak maximum by 2 nm from **Au-C1** to **Au-C2** is observed. These blue-shifts are attributed to the electron-withdrawing groups in **Au-C2** (4-CF_3-C_6H_4) and **Au-C3** (C_6F_5), leading to lowering of both the highest occupied molecular

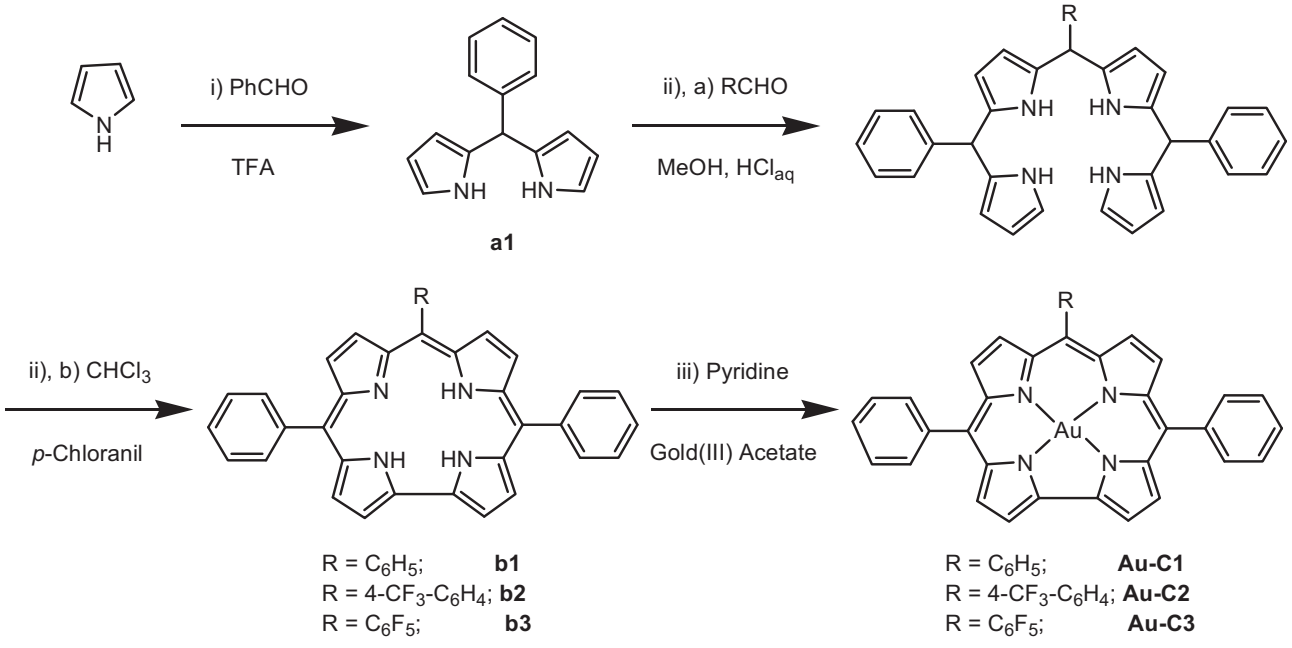

Scheme 1. Synthetic routes of **Au-C1**, **Au-C2**, and **Au-C3**. Reaction conditions: i) room temperature (r.t.), argon atmosphere (Ar), 1.2 hr; ii) a) r.t., Ar, 1 hr; ii) b) r.t., Ar, overnight; iii) r.t., Ar, 16 h.

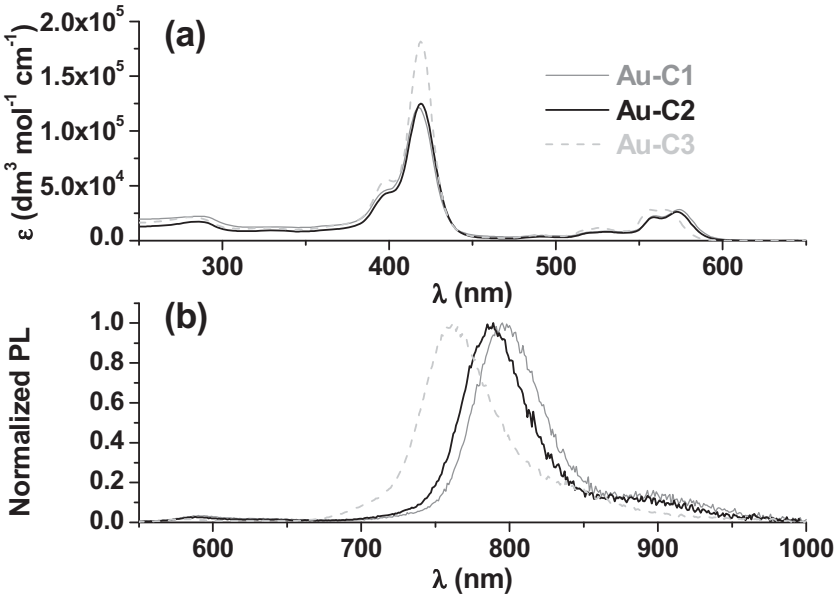

Figure 1. a) UV-vis absorption and b) normalized photoluminescence spectra of **Au-C**s in degassed dichloromethane (concentrations at 1.0×10^{-5} mol dm^{-3}) at 298 K.

orbital (HOMO) and the lowest unoccupied molecular orbital (LUMO). This spectral assignment is supported by the density functional theory (DFT) and time-dependent DFT (TDDFT) calculations with the molecular orbital (MO) diagrams further described below.

The emission spectra of **Au-C**s in DCM at room temperature are depicted in Figure 1b. The complexes exhibit emission bands in the region of 500 to 1000 nm. The low energy emissions of **Au-C**s at 761–796 nm with comparable Stokes shifts of ≈11 000 cm^{-1} are assigned to ligand-based phosphorescence as in the reported emissive metal-corroles.[45–47] Similar to the absorption energy, incorporation of fluorine atom/CF_3 group to the phenyl ring (s) causes a blue-shift in emission energy as revealed by the following order (emission wavelength): **Au-C1** (591, 796 nm) >**Au-C2** (588, 787 nm) >**Au-C3** (580, 761 nm). It is noteworthy that these **Au-C**s complexes have long excited lifetimes (≈24.9–107.1 µs) and low Φ_{PL} (0.03–0.12%) in degassed DCM at 298 K. Their long-lived excited states are anticipated to extend the exciton L_D that is beneficial for enhancing charge-collection and J_{SC}. The spectral data are summarized in **Table 1**. To further investigate the triplet excited state dynamics, nanosecond transient absorption (ns-TA) measurements were performed with these complexes in DCM solutions (1.0×10^{-5} mol dm^{-3}). The ns-TA spectra of **Au-C1**, **Au-C2**, and **Au-C3**, respectively, recorded at various time intervals after the photo-excitations at 355 nm, are given in ESI (Figure S7–S9). The ns-TA for **Au-C2** features a broad absorption band at 455 nm together with bleaching of the ground state absorption at the spectral region from 380 to 430 nm and from 545 to 590 nm. Analysis of the kinetic decay of the long-lived TA at 455 nm revealed a bi-exponential decay dynamics with decay time constants of approximately 69.6 and 22.4 µs.

The trend in photo-physical data is similar to corresponding trend of the electrochemical data. The HOMO and LUMO energies are derived from the oxidation and reduction potentials, respectively, both of which are measured by cyclic voltammetry (CV). The cyclic voltammograms of the **Au-C**s are shown in **Figure 2**. The HOMO/LUMO energy levels of **Au-C1**, **Au-C2**, and **Au-C3** were estimated to be –5.27/–3.04, –5.30/–3.07, –5.41/–3.13 eV, respectively, corresponding to the energy band-gap (E_{energy}) of 2.23, 2.23, 2.28 eV, respectively. As the E_{energy} values follow the same trend of E_{opt} values of the **Au-C**s, incorporation of fluorine atoms/CF_3 group to the corrole ligand increases both the reduction and oxidation potentials and downshifts the LUMO and HOMO levels with slight increase in the energy of HOMO-LUMO band-gap. As the maximum possible V_{OC} is governed by the energy offset between HOMO of donor and LUMO of acceptor, that is, $V_{OC} \approx e^{-1} \times (|HOMO_{Au\text{-}C}| - |LUMO_{C70}|)$, the energetically low-lying HOMO level of **Au-C**s may lead to an increase in V_{OC} of OSC, given that $HOMOs_{Au\text{-}C}$ are at –5.27, –5.30, and –5.41 eV for **Au-C1**, **Au-C2**, and **Au-C3**, $LUMO_{C70}$ is at –4.20 eV, and e is the elementary charge. It is noted that the energy difference between the LUMOs (or HOMOs) of **Au-C**s and C_{70} is about 1.1 eV (or 0.8 eV), thus providing sufficiently high driving force for exciton-dissociation at the hetero-junction interface.[9]

From the MO diagrams depicted in **Figure 3**, the energy levels of all the HOMOs and LUMOs decrease and the simulated HOMO-LUMO gap slightly increases from 1.78 to 1.86 eV on going from **Au-C1** to **Au-C3**. Based on TDDFT calculations, the absorption bands of **Au-C1**, **Au-C2**, and **Au-C3** are calculated at

Table 1. Physical data of **Au-C**s.

Material	UV-vis absorption[a] λ_{abs} [nm] (ε [×10^4 dm^3 mol^{-1} cm^{-1}])	λ_{PL} [nm]/τ [µs]/Φ_{PL} [%][a]	Red./Ox. $E_{1/2}$ [V][b] vs Fc/Fc$^+$	LUMO/HOMO [eV][c]	E_{energy}[d]/E_{opt}[e] [eV]	T_d[f] [°C]
Au-C1	287 (2.26), 418 (12.13), 559 (2.29), 574 (2.83)	796 / 24.9 / 0.03	–1.760 / 0.465	–3.04 / –5.27	2.23 / 2.10	357
Au-C2	285 (1.72), 419 (12.46), 559 (2.11), 572 (2.60)	787 / 63.1 / 0.04	–1.735 / 0.500	–3.07 / –5.30	2.23 / 2.11	355
Au-C3	281 (2.11), 419 (18.12), 556 (2.83), 566 (2.80)	761 / 107.1 / 0.12	–1.675 / 0.605	–3.13 / –5.41	2.28 / 2.13	371

[a]Determined in degassed dichloromethane solutions; [b]$E_{1/2} = (E_{pa} + E_{pc})/2$; E_{pa} and E_{pc} are the peak anodic and the peak cathodic potentials, respectively; [c]HOMO = $-e$ (E_{ox} + 4.8) eV; LUMO = $-e$(E_{red} + 4.8) eV; [d]Derived from oxidation and reduction potentials, respectively, determined by cyclic voltammetry; [e]Estimated from the absorption onset at the low energy side of absorption band; [f]5% weight loss in thermogravimetric analysis measurement. Heating rate: 10 °C min^{-1} under an ambient atmosphere.

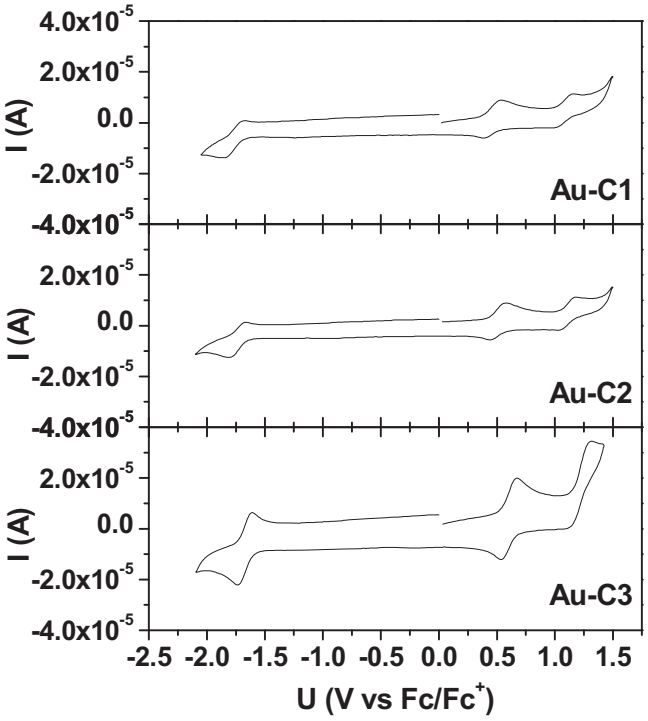

Figure 2. Cyclic voltammograms of **Au-C1**, **Au-C2**, and **Au-C3**.

573, 568, and 559 nm, respectively, which are in good agreement with the data from absorption spectra (574, 572, and 566 nm). The absorption of **Au-C1** at 573 nm is mainly attributed to HOMO→LUMO+1 (53%, LMCT) and HOMO→LUMO (33%, LLCT) transitions. The absorption of **Au-C2** at 568 nm is attributed to HOMO→LUMO+1 (40%, LMCT), HOMO→LUMO (30%, LLCT), and HOMO→LUMO+2 (16%, LLCT) transitions. The absorption of **Au-C3** at 559 nm is mainly attributed to HOMO→LUMO+2 (43%, LLCT), HOMO→LUMO (22%, LLCT), and HOMO→LUMO+1 (18%, LMCT) transitions. All of these absorption bands have mixed LMCT and LLCT characters;

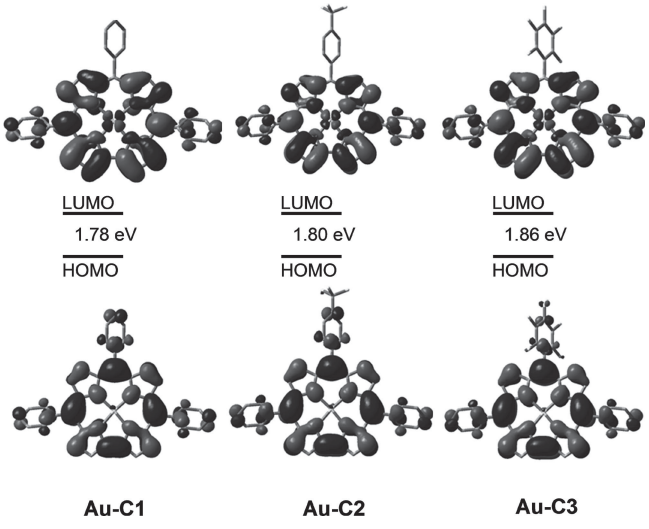

Figure 3. Molecular orbital (MO) diagrams of **Au-C1**, **Au-C2**, and **Au-C3** calculated at M06L/6-31G* (lanl2dz) level (isovalue = 0.02).

the LMCT character of the absorption decreases gradually from **Au-C1** to **Au-C3** (53% to 18%).

2.2. Au-Cs for OSCs

To explore the applicability of **Au-C**s as electron-donor, OSCs devices having the basic structure depicted in **Figure 4**a were fabricated via vacuum-deposition with **Au-C**s at different concentrations (x = 3%, 5%, and 7%) and C_{70} was used as electron-acceptor. A bulk hetero-junction (BHJ) with binary D–A interpenetrating network instead of planar hetero-junction was adopted because this has been proven to be a more efficient system for exciton-separation.[24,48] The BHJ provides a larger internal D–A interfacial area and is conceived to effectively suppress triplet-triplet annihilation (TTA)[49] that has commonly been encountered in organic semiconducting devices. For comparison, a C_{70}-only-cell has also been fabricated as reference. **Figure 5**a and **Table 2** depict the J–V characteristics and the key parameters of the PV devices based on **Au-C1** to **Au-C3**, respectively. The C_{70}-only-cell showed a poor PV response, that is, J_{SC} = 1.19 mA cm^{-2}; V_{OC} = 1.23 V; FF = 0.32; PCE = 0.5%. With **Au-C**s used as electron-donor, all PV responses have been dramatically improved. The OSCs with **Au-C1** and **Au-C2** showed superior PV responses (at their optimized concentrations of 7% and 5%, respectively). The devices based on **Au-C1** and **Au-C2** exhibited similar J_{SC} of 8.97 and 9.21 mA cm^{-2}, V_{OC} of 0.77 and 0.82 V, FF of 0.39 and 0.40, leading to the PCEs of 2.7% and 3.0%, respectively. With **Au-C3** used at an optimized concentration of 5%, a rather low PCE of 1.8% for the **Au-C3**-based OSC with J_{SC} and FF being 6.67 mA cm^{-2} and 0.30 respectively was obtained. This may be attributed to a poor carrier drift-mobility of **Au-C3**, as reflected from the high series resistance (R_S), that is, 649.7 Ω for **Au-C3**-based device, being much larger than that of 345.3 and 288.7 Ω for **Au-C1** and **Au-C2**-based devices. It is noted that an increase in V_{OC} has been observed, where V_{OC} of **Au-C1** (0.79 V) < **Au-C2** (0.82 V) < **Au-C3** (0.88 V). This is in good agreement with the HOMO energies for **Au-C1** (–5.27 eV) < **Au-C2** (–5.30 eV) < **Au-C3** (–5.41 eV), as the $V_{OC} \approx e^{-1} \times (|HOMO_{Au\text{-}C}| - |LUMO_{C70}|)$ (see **Figure 6** illustrating the energy level diagram[38,50,51] of the OSCs). The HOMO and LUMO values for both C_{70}[50] and bathophenanthroline (BPhen)[51] and the work functions for indium-tin-oxide (ITO)/MoO_x[38] and Al[51] were obtained from the literature.

After post-annealing treatment[6,48] under atmospheric conditions, the **Au-C1** and **Au-C2**-based OSCs showed enhanced PCEs of 3.4% and 4.0% (3.3% for **Au-C1** and 3.9% for **Au-C2** on average) under illumination using a standard AM1.5G simulated sunlight with an illumination power P_{in} of 100 mW cm^{-2}. Similar to other reported studies,[6,48] such improvement on PCE is ascribed to a better re-alignment of D–A molecules for enhancing absorption efficiency as well as increasing the D–A interface for exciton-dissociation and charge-transport properties.[48] Indeed, the conductivity of both **Au-C1** and **Au-C2**-based OSCs have been significantly enhanced after post-annealing in terms of reduced R_S of 250.9 and 210.7 Ω, respectively.

Figure 5b depicts the external quantum efficiency (EQE) spectra. The use of **Au-C** led to broadening of the spectral coverage as well as increased EQE of the devices. Particularly, the

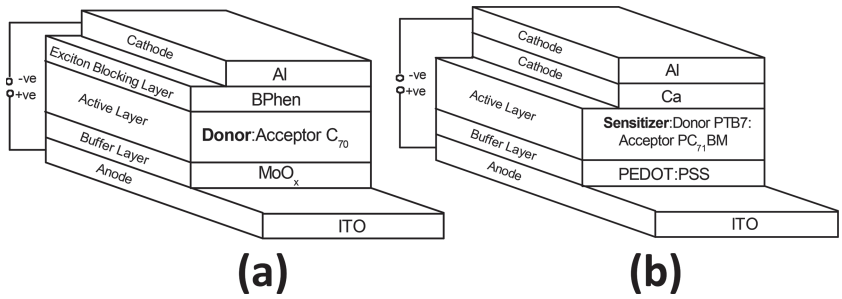

Figure 4. Basic device structures of a) vacuum-deposited and b) solution-processed organic solar cells.

plateau sensitivity of the **Au-C**-based devices covered the visible spectrum from 400 to 700 nm, the latter well-matched to the superposition of the absorption bands of C_{70} and **Au-C**. In addition, the average EQEs [peak] of **Au-C1** (post-annealed), **Au-C2** (post-annealed), **Au-C3**-based OSCs reached at ≈41% [71%], 45% [78%], 29% [51%], being much higher than that of the C_{70}-only-reference cell (i.e., 5% [22%]). The average EQEs [peak] of the **Au-C**-based devices are also comparable to those of the small molecular OSCs (as control devices) based on the best reported electron-donors of DIBSQ[1] (52% [73%]) and 1,1-*bis*-(4-*bis*(4-methyl-phenyl)-amino-phenyl)-cyclohexane (TAPC)[52] (39% [74%]), except that the DIBSQ-based OSC showed higher average EQE exceeding 50% with photo-response extending up to the near-infrared region at 800 nm. By integrating the EQE data,[19] the calculated J_{SC} values are given by the following Equation (1) and are consistent with the measured values acquired from *J–V* characteristics (within ±5% error):

$$J_{SC} = \int \frac{q\lambda}{hc} \mathrm{EQE}(\lambda) S(\lambda) \mathrm{d}\lambda \quad (1)$$

the constant term q/hc equals 8.0655×10^5 for wavelength in units of meters and $S(\lambda)$ is AM1.5G solar spectral density with an integrated intensity of 100 mW cm^{-2}.

The key PV parameters of the reported vacuum-deposited OSCs based on organometallic complexes[6,14–24] are summarized in **Table 3**. The PCE figures of the present OSCs based on **Au-C**s are the highest among the reported PCEs for vacuum-deposited OSCs incorporating triplet donor materials[6,14–24] and are comparable to those of the control OSCs based on the best reported electron-donors of DIBSQ[1] and TAPC[52] in combination with the electron-acceptor C_{70} prepared under the same processing conditions (see Table 2). It is worth noting that the J_{SC} of **Au-C2**-based device after post-annealing remained high at 10.34 mA cm^{-2} accompanying with high V_{OC} of 0.85 V. This observation is different from that of the *bis*(5,7-dimethyl-8-hydroxyquinolinato)platinum(II) ($Pt(Me_2q)_2$)[15] and *bis*(2-(4-tertbutylphenyl)benzothiazolato-*N*,*C*$^{2'}$)iridium(III)(acetylacetonate) ($((t\text{-}bt)_2Ir(acac)$)[19]-based devices reported in the literature, the latter two showed considerably high J_{SC} (i.e., 14.8 and 10.7 mA cm^{-2}) but rather low V_{OC} (i.e., 0.42 and 0.36 V) values, as shown in Table 3. The discrepancies may be the presence of molecular aggregation[5] and/or impurity, all of which could introduce trap states[17] thereby leading to lower V_{OC} in the later devices.

An outstanding feature of the **Au-C**s is their good solubility in common organic solvents. This is useful for solution-processed OSCs. To testify that the observed performance enhancement in OSCs is directly attributed to the use of **Au-C**, the PV responses of solution-processed OSCs with **Au-C2** doped in D–A conjugated polymers and with PTB7 and $PC_{71}BM$[53] used as electron-donor and electron-acceptor, respectively, were investigated. For comparison, an un-doped (gold-corrole-free) cell has also been fabricated as reference. Figure 4b shows the basic configuration of solution-processed OSCs. It was found that **Au-C2** could serve both as an electron-donor as well as sensitizer (simply termed **Au-C** as sensitizer for ternary OSC hereafter) in ternary OSCs,[54] in which cases large J_{SC} of 13.9 and 14.2 mA cm^{-2} for the non-treated and solvent-treated[55] OSCs respectively were obtained. These J_{SC} values were higher than that of the un-doped (i.e., PTB7:$PC_{71}BM$ only) reference device (J_{SC} = 13.2 mA cm^{-2}). Meanwhile, the **Au-C2**-doped device showed an enhanced EQE (i.e., average EQE of 53.6%) compared to that of 51.5% for un-doped OSC and eventually achieved a PCE of 6%,

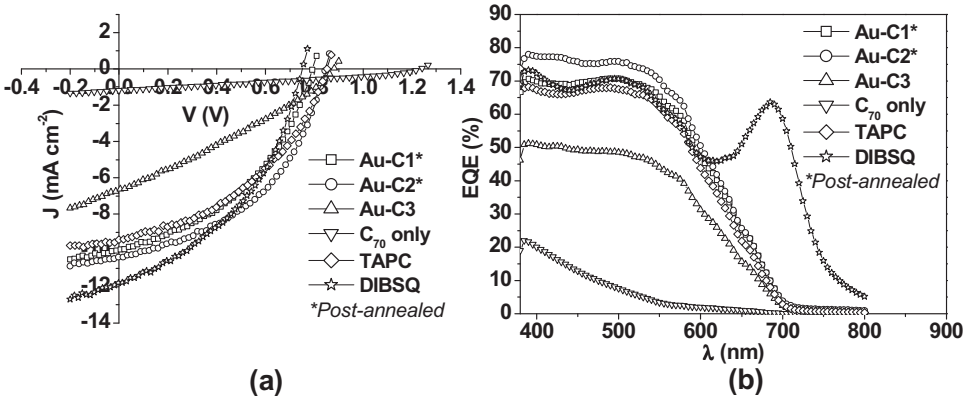

Figure 5. a) current density–voltage characteristics and b) the spectral photo-response of vacuum-deposited organic solar cells with **Au-C**s, C_{70} only (reference), TAPC (control), and DIBSQ (control), respectively, as donors and C_{70} as acceptor under AM1.5G illumination with an irradiation intensity of 100 mW cm^{-2} (P_{in} = 1 sun); the devices with **Au-C1** and **Au-C2** were post-annealed prior to the measurements.

Table 2. Photovoltaic performance parameters of the organic solar cells.

Active Layer	PCE @ P_{in} = 1 sun [%]	J_{SC} [mA cm^{-2}]	V_{OC} [V]	FF	R_S [Ω]
Au-C1 (3%): C_{70}[a,b]	1.1	4.09	0.80	0.34	870.2
Au-C1 (5%): C_{70}[a,b]	2.0	7.32	0.79	0.35	449.1
Au-C1 (7%): C_{70}[a,b]	2.7	8.97	0.77	0.39	345.3
Au-C1 (7%): C_{70}[a,b,c]	3.4	9.92	0.79	0.43	250.9
Au-C2 (3%):C_{70}[a,b]	2.5	8.11	0.84	0.36	437.5
Au-C2 (5%):C_{70}[a,b]	3.0	9.21	0.82	0.40	288.7
Au-C2 (7%):C_{70}[a,b]	2.9	8.92	0.80	0.41	254.7
Au-C2 (5%):C_{70}[a,b,c]	4.0	10.34	0.85	0.46	210.7
Au-C3 (3%): C_{70}[a,b]	1.5	5.79	0.90	0.29	869.9
Au-C3 (5%): C_{70}[a,b]	1.8	6.67	0.88	0.30	649.7
Au-C3 (7%): C_{70}[a,b]	1.6	6.34	0.85	0.29	628.6
C_{70} only[a,b] (Reference)	0.5	1.19	1.23	0.32	2134.5
TAPC:C_{70}[a,b] (Control)	3.3	9.37	0.85	0.42	280.0
DIBSQ:C_{70}[a,d] (Control)	3.7	11.77	0.75	0.42	205.5
Au-C2 (5%):PTB7:$PC_{71}BM$[e,f]	5.5	13.90	0.73	0.54	147.4
Au-C2 (5%):PTB7:$PC_{71}BM$[e,f,g]	6.0	14.18	0.74	0.57	136.9
PTB7:$PC_{71}BM$[e,f] (Reference)	5.3	13.22	0.73	0.55	146.8

[a]Vacuum-deposited small molecule-based; [b]ITO/MoO_x (2 nm)/Active Layer (60 nm)/BPhen (8 nm)/Al (100 nm); [c]Post-annealed; [d]ITO/MoO_x (4 nm)/Active Layer (60 nm)/BCP (10 nm)/Al (100 nm); [e]Solution-processed polymer-based; [f]ITO/PEDOT:PSS (30 nm)/Active Layer (80 nm)/Ca (20 nm)/Al (100 nm); [g]Solvent-treated. P_{in} is the power of the incident light.

as shown in **Figure 7** and Table 2. The present findings revealed that photon-harvesting process could be improved together with an increase in J_{SC} while V_{OC} remained unchanged by doping **Au-C2** in PTB7:$PC_{71}BM$. This is similar to the case of the ternary OSC with *fac-tris*(2-phenylpyridine)iridium(III) ($Ir(ppy)_3$) doped *N,N′-bis*(naphthalen-l-yl)-*N,N′-bis*(phenyl)-benzidine (NPD):fullerene (C_{60}) system previously reported by Luhman and Holmes,[22] where $Ir(ppy)_3$, NPD, and C_{60} were used as sensitizer, donor, and acceptor, respectively. Xu et al.[56] also reported that the recombination of dissociated charge carriers could be suppressed when $Ir(ppy)_3$ was dispersed into poly(2-methoxy-5-(2′-ethylhexyloxy)-1,4-phenylenevinylene)

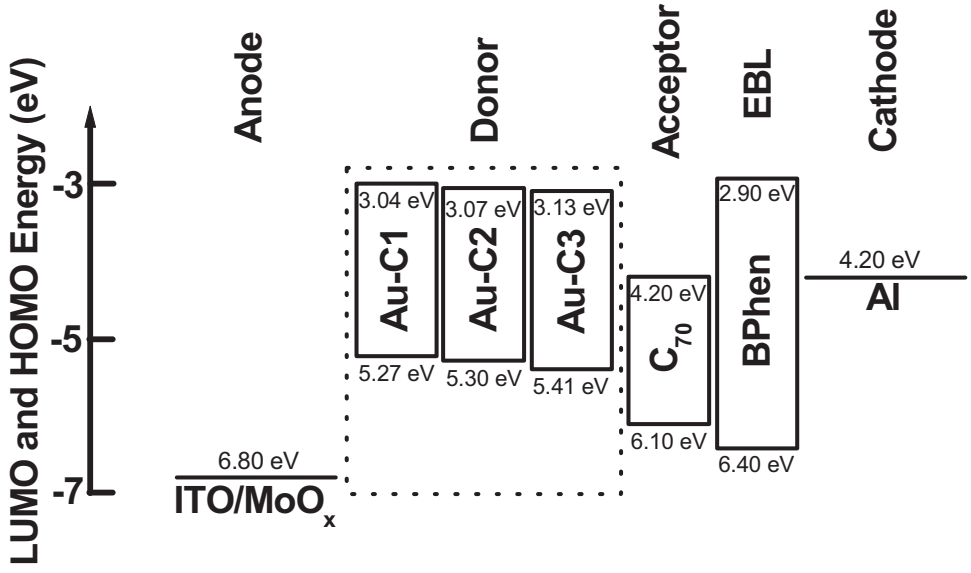

Figure 6. Schematic energy level diagram of the organic solar cells. LUMO and HOMO are the lowest unoccupied molecular orbital and the highest occupied molecular orbital, respectively. EBL is the exciton blocking layer.

Table 3. Summary of photovoltaic parameters of vacuum-deposited organic solar cells based on organometallic compounds reported in the literature.

Active Layer	PCE [%]	J_{SC} [mA cm^{-2}]	V_{OC} [V]	FF	Refs.
Au-C2 (5%):C_{70}	4.0	10.34	0.85	0.46	This work
Au-C1 (7%): C_{70}	3.4	9.92	0.79	0.43	This work
Au-C3 (5%): C_{70}	1.7	6.67	0.88	0.30	This work
AP**Ir**/C_{60}	2.8	4.50	0.99	0.62	[14]
Pt$(Me_2q)_2$/C_{60}	2.4	14.80	0.42	0.38	[15]
$(pbi)_2$**Ir**(acac)/C_{60}	2.3	4.82	0.78	0.60	[16]
PdPc/C_{60}	2.2	6.80	0.57	0.57	[17]
PtOEP/C_{60}	2.1	5.60	0.66	0.57	[6]
PtTPBP/C_{60}	1.9	4.48	0.69	0.63	[18]
Pentacene/$(t\text{-bt})_2$**Ir**(acac)/C_{60}	1.9	10.70	0.36	0.48	[19]
PdTPBP/C_{60}	1.8	4.31	0.65	0.64	[18]
PtOEP (5%):SY/C_{60}	1.6	3.50	0.86	0.52	[20]
$(t\text{-bt})_2$**Ir**(acac) (25%):CuPc/C_{60}	1.4	8.23	0.36	0.47	[21]
Ir$(ppy)_3$ (5%):NPD/C_{60}	1.3	—	—	—	[22]
Pt-8C_4-TPP:P3HT/C_{60}	0.7	4.15	0.41	0.41	[23]
CuPc/2 (**Ir**) (20%):C_{60}/C_{60}	0.6	2.32	0.49	0.53	[24]
Pt-8C_4-TPP/C_{60}	0.1	0.37	0.38	0.32	[23]

(MEH-PPV):$PC_{61}BM$ system. These workers showed that the employment of compounds containing light metal atom as electron-donor/sensitizer, for example, *tris*(8-hydroxyquinoline) aluminum (Alq_3), led to poor OSC performance.[56] This may be due to the weak spin-orbital coupling in the case of Alq_3, although both Ir$(ppy)_3$ and Alq_3 have similar HOMO and LUMO energies.[56] Nevertheless, the results obtained with the **Au-C2**-devices are among the best for all of the reported solution-processed polymer-based OSCs using metal-organic complexes as electron-donor/sensitizer. The key PV parameters of solution-processed polymer-based OSCs based on the metal-organic complexes reported in the literature[7,24–34] are depicted in **Table 4**.

In literature, the metal-organic complexes used in the development of OSCs are mainly confined to the ones of iridium,[14,16,19,21,22,24,29,33,34] platinum,[6,7,15,18,20,23,25–28,31] palladium,[17,18] rhenium,[30] and ruthenium,[32] all of which are known to have luminescent triplet excited states. To our knowledge, there is no report on the use of gold(III) complexes for OSCs despite the fact that gold is the heaviest one among the transition metals aforementioned and is therefore expected to have a strong spin-orbit coupling effect.[17] The present work is the first report on OSCs fabricated with gold(III) complexes as electron-donor/sensitizer.

The superior performance of OSCs based on **Au-C**s may be correlated to their considerably low Φ_{PL} value, the latter favors a higher rate of dissociation of excitons (k_d). It is noted that exciton-dissociation is needed for the generation of photocurrent. A schematic diagram illustrating the mechanisms of photoconversion occurring in OSC utilizing the triplet excited state of photoactive material is depicted in **Figure 8**. Under light-illumination, the photoactive material absorbs the energy of incident light photon leading to the formation of excitons. These excitons will diffuse to the D–A interface where the electron-hole pairs undergo dissociation. For the materials with accessible long-lived triplet excited state(s), singlet-triplet transition through ISC takes place. These photo-generated excitons then dissociate into free charges leaving holes in the donor and electrons in the acceptor. The separated holes and electrons will migrate towards the respective electrodes, contributing to the photocurrent. Excitons that do not reach the interface within their lifetimes will undergo either via i) non-radiative decay with the liberation of heat or ii) radiative decay with light-emission. The total EQE of OSCs can be expressed as the direct product of three components: $\eta_{Total} = \eta_A\eta_{ED}\eta_{CC}$, where η_A, η_{ED}, and η_{CC} are the light-absorption, the exciton-dissociation, and the charge-collection efficiencies, respectively. It should be highlighted that the two decay channels [i.e., (i) and (ii)] of excitons would compete with iii) exciton-dissociation process in the dissipation of photo-generated excitons. Thus adopting weakly emissive metal complexes having long-lived excited state(s) may favor exciton-dissociation thereby leading to increase of the photocurrent. One would expect that k_d can be increased by suppressing the radiative decay channel (i.e., decrease in radiative decay rate constant (k_r)) via the use of weakly emissive electron-donor. In order to shed insight into the factor(s) affecting the device performance, the solution Φ_{PL} of **Au-C1**, **Au-C2**, and **Au-C3** have been measured. Interestingly, all the **Au-C**s are weakly emissive, that is, their Φ_{PL} are only 0.03%, 0.04%, and 0.12% respectively. As aforementioned, most of the reported luminescent metal-organic/organometallic complexes used in OSCs are excellent phosphorescent emitters with examples including 2,3,7,8,12,13,17,18-octaethyl-21*H*,23*H*-porphineplatinum(II) (PtOEP),[6,20] *bis*(1,2-diphenyl-1*H*-benzoimidazole)iridium(III)(acetylacetonate) ($(pbi)_2$Ir(acac)),[16] and Ir$(ppy)_3$,[22] having remarkably high Φ_{PL}

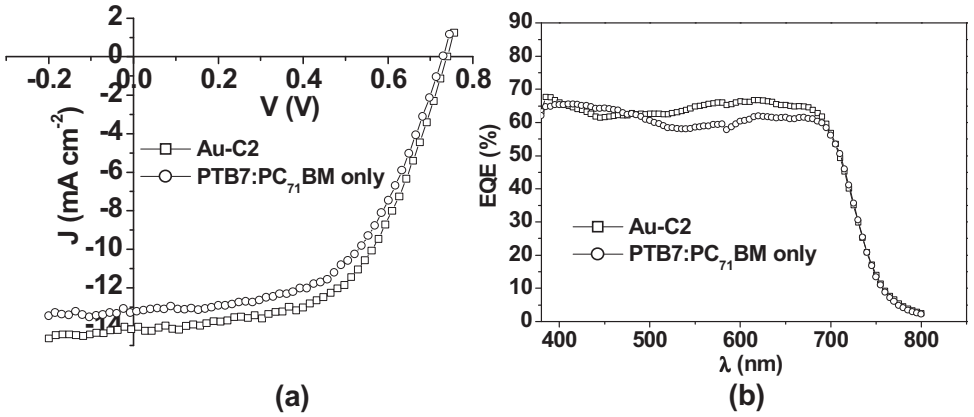

Figure 7. a) current density–voltage characteristics and b) the spectral response of solution-processed polymer-based organic solar cells without (reference), i.e., PTB7:$PC_{71}BM$ only, and with **Au-C2** as the sensitizer under AM1.5G illumination with an irradiation intensity of 100 mW cm^{-2} (1 sun). PTB7 acted as electron-donor and $PC_{71}BM$ acted as electron-acceptor.

and long emission lifetimes (Φ_{PL} are 42%, 73%, and 73% and the lifetimes are 50, 2, and 1 μs for PtOEP,[57] $(pbi)_2Ir(acac)$,[58] and $Ir(ppy)_3$[59] in deaerated toluene solutions). In this work, the less emissive behavior of **Au-C**s having low Φ_{PL} results in lower k_r and thus higher k_d values. This may account for the PCEs of the present **Au-C**-based OSCs being much higher than those of OSCs fabricated with the other highly luminescent metal complexes. In literature, a high concentration of $Ir(ppy)_3$ up to 25 mol% was used in the OSCs.[33] Such a high concentration of the $Ir(ppy)_3$ electron-donor can effectively induce concentration self-quenching and avoids the recombination loss through radiative decay of the triplet excited state of $Ir(ppy)_3$. Inset in Figure 8 shows a photograph of the prototypical module for large area (≈1 cm^2) OSC incorporating the donor of **Au-C2** and the acceptor of C_{70}.

3. Conclusion

In this work, high performance OSCs comprising the **Au-C**s, that is, **Au-C1**, **Au-C2**, and **Au-C3**, as electron-donor in combination with C_{70} as acceptor have been fabricated. These **Au-C**s have long excited state τ_t of ≥ 25 μs as well as low Φ_{PL} of < 0.15%. In addition, they have a good solubility in common organic solvents and can be utilized in solution-processed OSCs. Vacuum-deposited OSCs based on **Au-C1**, **Au-C2**, and **Au-C3** gave PCEs of 2.7%, 3.0%, and 1.8%, under illumination using 1 sun standard AM1.5G simulated sunlight; the PCE could be further improved after post-annealing. The highest PCEs of 4.0% and 6.0% could be realized in both optimized vacuum-deposited and solution-processed OSCs based on **Au-C2**. The present results revealed that **Au-C**s are a promising class

Table 4. Summary of photovoltaic parameters of solution-processed polymer-based organic solar cells based on organometallic compounds reported in the literature.

Active Layer	PCE [%]	J_{SC} [mA cm^{-2}]	V_{OC} [V]	FF	Refs.
Au-C2 (5%):PTB7:$PC_{71}BM$	6.0	14.18	0.74	0.57	This work
P1 (**Pt**) (20%):$PC_{61}BM$	4.9	15.43	0.82	0.39	[25]
BTD-**Pt**-T3 (20%):$PC_{71}BM$	3.0	8.45	0.82	0.43	[26]
P3 (**Pt**) (15%):$PC_{61}BM$	2.7	6.40	0.90	0.46	[27]
p-**Pt**BTD-Th (20%):$PC_{61}BM$	1.4	7.17	0.54	0.36	[28]
Ir(btpy)$_3$ (2%):P3HT:$PC_{61}BM$	1.0	4.25	0.59	0.38	[29]
bpy-DPA-TSB-**Re** (50%):$PC_{61}BM$	0.8	3.80	0.75	0.28	[30]
CuPc/2 (**Ir**) (20%):$PC_{61}BM/C_{60}$	0.5	2.65	0.44	0.43	[24]
P1 (**Pt**) (20%):$PC_{61}BM$	0.4	1.40	0.78	0.32	[31]
p-**Pt**Th (20%):$PC_{61}BM$	0.3	0.99	0.64	0.43	[7]
2 (**Ru**) (30%):$PC_{61}BM$	0.1	0.66	0.40	0.31	[32]
2 (**Ir**) (20%):$PC_{61}BM$	0.1	0.44	0.63	0.19	[33]
Ir(mppy)$_3$ (10%):P3HT:CdSe	—	0.06	0.85	—	[34]

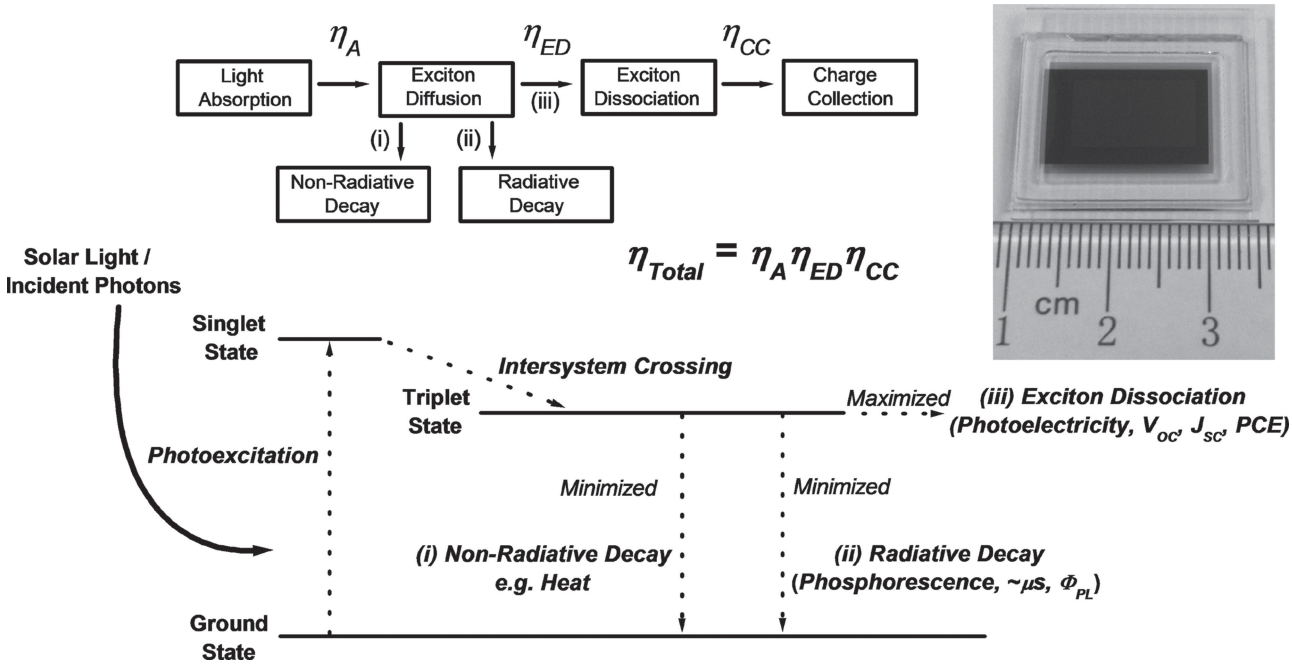

Figure 8. Mechanisms of photoconversion in organic solar cells with triplet photoactive materials. η_{Total}, η_A, η_{ED}, and η_{CC} are the total, light-absorption, exciton-dissociation and charge-collection efficiencies, respectively. Inset shows a photograph of the prototypical module for large area (≈1 cm^2) organic solar cell incorporating the **Au-C2** donor and C_{70} acceptor.

of electron-donors for use in OSCs. With judicious choice of metal ion and auxiliary ligand(s), it may be feasible to realize efficient OSCs based on organometallic complexes having accessible long-lived triplet excited states.

4. Experimental Section

Material Synthesis and Characterization: All chemicals used for syntheses were purchased from Sigma-Aldrich Chemical Co. The **Au-C**s, that is, **Au-C1**, **Au-C2**, and **Au-C3** were prepared according to literature procedures.[41–44]

a1 *(5-Phenyldipyrromethane)*: A mixture of pyrrole (0.2 mol, 14 mL) and benzaldehyde (10 mmol, 1 mL) was added to a dried 100 mL round-bottomed flask and degassed with a stream of Ar for 5 min. Trifluoroacetic acid (TFA) (1 mmol, 0.08 mL) was added. The resulting solution was stirred for about 1 h 20 min at ambient temperature followed by quenching with addition of sodium hydroxide (NaOH) (0.1 M, 3 mL). The mixture was extracted with ethyl acetate. The organic phase was washed with distilled water and dried by anhydrous sodium sulphate (Na_2SO_4). After removal of solvent, the crude product was purified by column chromatography with eluent of dichloromethane (CH_2Cl_2) : hexane (v/v = 1/2). A yellow solid was obtained (1.45 g, 66%).

b1 *(5,10,15-Triphenylcorrole)*: A mixture of **a1** (2 mmol, 444 mg) and benzaldehyde (1 mmol, 0.1 mL) was dissolved in a mixture of methanol (MeOH) (75 mL), H_2O (75 mL), and 36% hydrochloric acid (HCl_{aq}) (5 mL). The resultant mixture was stirred at ambient temperature for 1 h. Chloroform ($CHCl_3$) was added for extraction. The organic layer was washed twice with H_2O, and dried by Na_2SO_4. After filtration, the filtrate was diluted with $CHCl_3$ to 250 mL. Then *p*-Chloranil (3 mmol, 738 mg) was added, and the resulting mixture was stirred overnight at ambient temperature. The crude product was purified by column chromatography with eluent of CH_2Cl_2 : hexane (v/v = 1:1). A green-violet solid was obtained (100 mg, 20%). FAB-MS: *m/z* 562.2 [M^+].

Au-C1 *(Gold(III) 5,10,15-Triphenylcorrole)*: A mixture of **b1** (0.152 mmol, 80 mg), gold(III) acetate (0.76 mmol, 284 mg), and pyridine (8 mL) was stirred for 16 h. The pyridine was removed by rotatory evaporation. Chromatography of the reaction mixture on silica gel column with eluent of CH_2Cl_2 : hexane (v/v = 1/4) gave the product (5 mg, 4%). ^{1}H NMR (400 MHz, $CDCl_3$) δ = 9.21 (d, *J* = 4.5, 2H), 9.05 (d, *J* = 4.9, 2H), 8.88 (d, *J* = 4.5, 2H), 8.81 (d, *J* = 4.9, 2H), 8.30 (d, *J* = 6.7, 4H), 8.20 (d, *J* = 7.7, 2H), 7.85-7.73 (m, 9H). FAB-MS: *m/z* 720.1 [M^+].

b2 *(10-(p-trifluoromethylphenyl)-5,15-diphenylcorrole)*: Prepared with procedure similar to **b1** using 4-(trifluoromethyl)benzaldehyde ((1 mmol) instead of benzaldehyde. A green-violet solid was obtained (180 mg, 29%). FAB-MS: *m/z* 594.1 [M^+].

Au-C2 *(Gold(III) 10-(p-trifluoromethylphenyl)-5,15-diphenylcorrole)*: Prepared from **b2** (0.287 mmol), gold(III) acetate (0.8 mmol) and pyridine (8 mL) with the synthetic procedure of **Au-C1**. The product was purified by chromatography on silica gel column with eluent of CH_2Cl_2 : hexane (v/v = 1/8). A deep red solid was obtained (60 mg, 27%). ^{1}H NMR (400 MHz, $CDCl_3$) δ = 9.21 (d, *J* = 4.5, 2H), 9.06 (d, *J* = 4.9, 2H), 8.89 (d, *J* = 4.5, 2H), 8.74 (d, *J* = 4.9, 2H), 8.31 (s, 2H), 8.29 (d, *J* = 6.8, 4H), 8.05 (s, 2H), 7.86-7.74 (m, 6H). FAB-MS: *m/z* 788.1 [M^+]

b3 *(10-(pentafluorophenyl)-5,15-diphenylcorrole)*: Prepared from 2,3,4,5,6-pentafluorobenzaldehyde(1 mmol) using the synthetic procedure of **b1**. A green-violet solid was obtained (154 mg, 25%). EI-MS: *m/z* 616.1 [M^+].

Au-C3 *(Gold(III) 10-(pentafluorophenyl)-5,15-diphenyl-corrole)*: Prepared from **b3** (0.13 mmol), gold(III) acetate (0.67 mmol), and pyridine (8 mL) by using the synthetic procedure of **Au-C2**. The product was purified by chromatography on silica gel column with eluent of CH_2Cl_2 : hexane (v/v = 1/8). A purple solid was obtained (30 mg, 29%). ^{1}H NMR (400 MHz, $CDCl_3$) δ = 9.20 (d, *J* = 4.5, 2H), 9.11 (d, *J* = 4.9, 2H), 8.89 (d, *J* = 4.5, 2H), 8.67 (d, *J* = 4.8, 2H), 8.29 (d, *J* = 6.4, 4H), 7.86-7.74 (m, 6H). FAB-MS: *m/z* 810.1 [M^+].

^{1}H NMR spectra were recorded using $CDCl_3$ as solvent on a Bruker Avance 400 Fourier-Transform NMR spectrometer; chemical shifts were reported relative to tetramethylsilane (Solvents: $CDCl_3$; DMSO-d_6 and CD_2Cl_2; chemical shifts: δ, ppm; *J*, Hz). Positive ion fast atom bombardment mass spectrometry (FAB-MS) was performed on a Finnigan MAT 95 mass spectrometer. Photo-excitation and steady-state emission spectra were obtained on a SPEX Fluorolog-3 Model

FL3-21 spectrofluorometer. UV-vis absorption spectra were recorded on a Hewlett-Packard 8452A diode array spectrophotometer. Φ_{PL} values were measured relative to that of a degassed acetonitrile solution of $[Ru(bpy)_3]$ $(PF_6)_2$ (bpy = 2,2′-bipyridine) (Φ_{ref} = 0.062) as a standard reference and calculated by: $\Phi_s = \Phi_r$ (B_r/B_s) $(n_s/n_r)^2$ (D_s/D_r), where the subscripts *s* and *r* refer to sample and reference standard solutions, respectively, *n* is the refractive index of the solvents, *D* is the integrated intensity, and Φ is the luminescence quantum yield. The excitation intensity *B* was calculated by: $B = 1 - 10^{-AL}$, where *A* is the absorbance at the excitation wavelength and *L* is the optical path length ($L = 1$ cm in all cases). Energies of HOMO and LUMO levels of the organic materials were estimated from the oxidation and reduction potentials measured by cyclic voltammetry. A conventional two-compartment electrochemical cell was used. The glassy-carbon electrode was polished with 0.05 μm alumina on a microcloth, sonicated for 5 min in deionized water, and rinsed with acetonitrile prior to use. An $Ag/AgNO_3$ (0.1 M in CH_3CN) electrode was used as reference electrode and a platinum wire as counter electrode. All solutions of samples were prepared in dichloromethane (HPLC grade and degassed with nitrogen gas prior to use) with 0.1 mol dm^{-3} tetra(*n*-butyl)ammonium hexafluorophosphate ($TBAPF_6$) as supporting electrolyte. All potentials were referenced to Fc/Fc^+ ($Cp_2Fe^{+/0}$) couple (–4.80 eV versus vacuum). The ns-TA measurements were performed with a LP920-KS Laser Flash Photolysis Spectrometer (Edinburgh Instruments Ltd., Livingston, UK). The excitation light source was the 355 nm output (third harmonic) of a Nd:YAG laser (Spectra-Physics Quanta-Ray Lab-130 Pulsed Nd:YAG Laser). A Hamamatsu R928 photomultiplier tube was used. The signals were processed by a PC plug-in controller with L900 software. TGA measurements were performed with a Perkin-Elmer TGA 7 thermogravimetric analyzer.

Computational Details: DFT and TDDFT calculations were performed using a basis set of 6-31G*[60] for C, H, O and N atoms, and effective core potential (ECP) lanl2dz[61] was used for the gold atom. The geometries of complexes **Au-C1**–**Au-C3** were calulated and optimized with B3LYP,[62–65] M06,[66] M06L,[67] M06-2X,[66] PBE0,[68] tHCTH,[69] and TPSSh functionals, and the findings were compared with the reported structural data of gold-corrole.[70] TDDFT calculations were performed based on the optimized geometries of complexes **Au-C1** to **Au-C3**. The polarizable continuum model (PCM)[71,72] for dichloromethane was chosen as the solvation model to simulate the solvation effect. The simulated energy levels of HOMO and LUMO and the corresponding energy gaps between HOMO and LUMO of complexes were calculated, and the frontier molecular orbital (FMO) surfaces were created for analysis.

OSC Fabrication and Characterization: Poly(3,4-ethylenedioxythiophene):polystyrenesulfonate (PEDOT:PSS), fullerenes, PTB7, and BPhen acquired from Bayer AG, American Dye Source Inc., 1-Material Chemscitech Inc., and e-Ray Optoelectronics Technology Co., Ltd, respectively, were used as received. OSCs were grown on glass substrates pre-coated with an anode of ITO with sheet resistance of 15 Ohm $square^{-1}$. They were cleaned in organic solvents, Decon 90 detergent, and deionized water[73–75] under ultrasonication and subsequently dried in oven and were subjected to ultraviolet ozone treatment prior to film deposition. For solution-processed polymer-based OSCs, a ≈30 nm anode buffer layer of PEDOT:PSS (Baytron P VP A1 4083) was spin-coated onto the ITO surface and baked in air at 150 °C for 5 min in order to remove the residual solvent. A blend of active layer **Au-C**:PTB7:$PC_{71}BM$ (1:9:15 by weight), with a thickness of ≈80 nm, was cast on PEDOT:PSS from a solution (concentration: 25 mg mL^{-1}) in chlorobenzene/1,8-diiodooctane (97:3% by volume) mixed solvent. The samples were immediately loaded into an evaporator where a top composite cathode layer consisting of calcium (20 nm) and aluminum (100 nm) was deposited under high vacuum ($<5 \times 10^{-6}$ Torr). For vacuum-deposited OSCs, a 2 nm anode buffer layer of MoO_x, a 60 nm blend of active layer containing **Au-C** donor and C_{70} acceptor, an 8 nm exciton blocking layer of BPhen,[74,75] and a 100 nm top cathode of aluminum, were sequentially deposited onto the cleaned and ultraviolet-treated ITO surface in the vacuum evaporator. MoO_x was used as the Schottky barrier contact to the photoactive layer.[38,52] The ratio of donor and acceptor in the blend of active layer was controlled by independently varying their deposition rates. All organic and metal layers were successively deposited at a rate of 0.1–0.2 nm s^{-1} in a Trovato Mfg., Inc. high vacuum evaporator under a base pressure of $< 5 \times 10^{-6}$ Torr without vacuum break. Film thicknesses were determined in-situ by calibrated oscillating quartz-crystal sensors. Shadow masks were used to define the patterns of organic and cathode layers to make four 0.1 cm^2 devices on each substrate. An ORIEL 300 W Xenon lamp equipped with an AM1.5G filter was used as a solar simulator to provide an illumination with an incident power of 100 mW cm^{-2} (1 sun) for both types OSCs. The illumination intensity was calibrated by an ORIEL crystal silicon reference diode with KG-5 visible color filter. Electrical *J*–*V* characteristics were measured with a programmable Keithley model 2400 source-meter measurement unit. For EQE (also called spectral photoresponse) measurements, OSCs were irradiated with monochromatic light of variable wavelength (from 380 to 800 nm with an interval of 5 nm) using an Oriel Cornerstone 260 monochromator with a 300 W Xenon arc lamp as the light source. The intensity of the source at each wavelength was determined using a calibrated silicon detector. The photocurrent under short-circuit conditions was recorded by using a dual channel radiometer at 10 nm intervals for each device. All experiments and measurements were carried out at room temperature under ambient environment without device encapsulation.

Supporting Information

Supporting Information is available from the Wiley Online Library or from the author.

Acknowledgements

S.L.L. and L.W. contributed equally to this work. This work was supported by the Theme-Based Research Scheme (T23-713/11), the Innovation and Technology Commission of the HKSAR Government (ITS/310/11), and the National Key Basic Research Program of China (No. 2013CB834802). The authors thank Pui-Kei Lee for material synthesis and Wai-Pong To for ns-TA measurements.

Received: January 10, 2014
Revised: February 25, 2014
Published online: April 22, 2014

[1] G. Chen, H. Sasabe, Z. Wang, X. F. Wang, Z. Hong, Y. Yang, J. Kido, *Adv. Mater.* **2012**, *24*, 2768.
[2] Z. He, C. Zhong, S. Su, M. Xu, H. Wu, Y. Cao, *Nat. Photonics* **2012**, *6*, 591.
[3] J. You, C. C. Chen, Z. Hong, K. Yoshimura, K. Ohya, R. Xu, S. Ye, J. Gao, G. Li, Y. Yang, *Adv. Mater.* **2013**, *25*, 3973.
[4] J. You, L. Dou, K. Yoshimura, T. Kato, K. Ohya, T. Moriarty, K. Emery, C. C. Chen, J. Gao, G. Li, Y. Yang, *Nat. Commun.* **2013**, *4*, 1446.
[5] a) A. Mishra, P. Bäuerle, *Angew. Chem.* **2012**, *124*, 2060; b) *Angew. Chem. Int. Ed.* **2012**, *51*, 2020.
[6] Y. Shao, Y. Yang, *Adv. Mater.* **2005**, *17*, 2841.
[7] F. Guo, Y. G. Kim, J. R. Reynolds, K. S. Schanze, *Chem. Commun.* **2006**, *2006*, 1887.
[8] Z. He, C. Zhong, X. Huang, W. Y. Wong, H. Wu, L. Chen, S. Su, Y. Cao, *Adv. Mater.* **2011**, *23*, 4636.
[9] S. L. Lai, M. F. Lo, M. Y. Chan, C. S. Lee, S. T. Lee, *Appl. Phys. Lett.* **2009**, *95*, 153303.
[10] F. R. Dai, H. M. Zhan, Q. Liu, Y. Y. Fu, J. H. Li, Q. W. Wang, Z. Xie, L. Wang, F. Yan, W. Y. Wong, *Chem. Eur. J.* **2012**, *18*, 1502.
[11] L. Liu, C. L. Ho, W. Y. Wong, K. Y. Cheung, M. K. Fung, W. T. Lam, A. B. Djurišić, W. K. Chan, *Adv. Funct. Mater.* **2008**, *18*, 2824.
[12] N. Chawdhury, A. Köhler, R. H. Friend, W. Y. Wong, J. Lewis, M. Younus, P. R. Raithby, T. C. Corcoran, M. R. A. Al-Mandhary, M. S. Khan, *J. Chem. Phys.* **1999**, *110*, 4963.

[13] W. Y. Wong, C. L. Ho, *Acc. Chem. Res.* **2010**, *43*, 1246.
[14] T. B. Fleetham, Z. Wang, J. Li, *Inorg. Chem.* **2013**, *52*, 7338.
[15] K. H. Low, Z. X. Xu, H. F. Xiang, S. S. Y. Chui, V. A. L. Roy, C. M. Che, *Chem. Asian J.* **2011**, *6*, 3223.
[16] N. Wang, J. Yu, Y. Zheng, Z. Guan, Y. Jiang, *J. Phys. Chem. C* **2012**, *116*, 5887.
[17] I. Kim, H. M. Haverinen, Z. Wang, S. Madakuni, Y. Kim, J. Li, G. E. Jabbour, *Chem. Mater.* **2009**, *21*, 4256.
[18] M. D. Perez, C. Borek, P. I. Djurovich, E. I. Mayo, R. R. Lunt, S. R. Forrest, M. E. Thompson, *Adv. Mater.* **2009**, *21*, 1517.
[19] J. Huang, J. Yu, Z. Guan, Y. Jiang, *Appl. Phys. Lett.* **2010**, *97*, 143301.
[20] B. P. Rand, S. Schols, D. Cheyns, H. Gommans, C. Girotto, J. Genoe, P. Heremans, J. Poortmans, *Org. Electron.* **2009**, *10*, 1015.
[21] J. Yu, J. Huang, H. Lin, Y. Jiang, *J. Appl. Phys.* **2010**, *108*, 113111.
[22] W. A. Luhman, R. J. Holmes, *Appl. Phys. Lett.* **2009**, *94*, 153304.
[23] Y. Li, R. Mastria, K. Li, A. Fiore, Y. Wang, R. Cingolani, L. Manna, G. Gigli, *Appl. Phys. Lett.* **2009**, *95*, 043101.
[24] W. Lee, T. H. Kwon, J. Kwon, J. Y. Kim, C. Lee, J. I. Hong, *New J. Chem.* **2011**, *35*, 2557.
[25] W. Y. Wong, X. Z. Wang, Z. He, A. B. Djurisic, C. T. Yip, K. Y. Cheung, H. Wang, C. S. K. Mak, W. K. Chan, *Nat. Mater.* **2007**, *6*, 521.
[26] X. Zhao, C. Piliego, B. Kim, D. A. Poulsen, B. Ma, D. A. Unruh, J. M. J. Fréchet, *Chem. Mater.* **2010**, *22*, 2325.
[27] W. Y. Wong, X. Z. Wang, Z. He, K. K. Chan, A. B. Djurišić, K. Y. Cheung, C. T. Yip, A. M. C. Ng, Y. Y. Xi, C. S. K. Mak, W. K. Chan, *J. Am. Chem. Soc.* **2007**, *129*, 14372.
[28] J. Mei, K. Ogawa, Y. G. Kim, N. C. Heston, D. J. Arenas, Z. Nasrollahi, T. D. McCarley, D. B. Tanner, J. R. Reynolds, K. S. Schanze, *ACS Appl. Mater. Interfaces* **2009**, *1*, 150.
[29] Z. Wang, F. Zhang, *Int. J. Photoenergy* **2013**, *2013*, 273586.
[30] F. He, Y. Zhou, S. Liu, L. Tian, H. Xu, H. Zhang, B. Yang, Q. Dong, W. Tian, Y. Ma, J. Shen, *Chem. Commun.* **2008**, *2008*, 3912.
[31] L. Li, W. C. Chow, W. Y. Wong, C. H. Chui, R. S. M. Wong, *J. Organomet. Chem.* **2011**, *696*, 1189.
[32] A. Colombo, C. Dragonetti, D. Roberto, R. Ugo, L. Falciola, S. Luzzati, D. Kotowski, *Organometallics* **2011**, *30*, 1279.
[33] G. L. Schulz, S. Holdcroft, *Chem. Mater.* **2008**, *20*, 5351.
[34] C. M. Yang, C. H. Wu, H. H. Liao, K. Y. Lai, H. P. Cheng, S. F. Horng, *Appl. Phys. Lett.* **2007**, *90*, 133509.
[35] L. Xiao, Z. Chen, B. Qu, J. Luo, S. Kong, Q. Gong, J. Kido, *Adv. Mater.* **2011**, *23*, 926.
[36] Y. Chi, P. T. Chou, *Chem. Soc. Rev.* **2010**, *39*, 638.
[37] a) P. K. Chow, C. Ma, W. P. To, G. S. M. Tong, S. L. Lai, S. C. F. Kui, W. M. Kwok, C. M. Che, *Angew. Chem.* **2013**, *125*, 11991; b) *Angew. Chem. Int. Ed.* **2013**, *52*, 11775.
[38] S. L. Lai, W. Y. Tong, S. C. F. Kui, M. Y. Chan, C. C. Kwok, C. M. Che, *Adv. Funct. Mater.* **2013**, *23*, 5168.
[39] X. Z. Wang, Q. Wang, L. Yan, W. Y. Wong, K. Y. Cheung, A. Ng, A. B. Djuriši , W. K. Chan, *Macromol. Rapid Commun.* **2010**, *31*, 861.
[40] C. Qin, Y. Fu, C. H. Chui, C. W. Kan, Z. Xie, L. Wang, W. Y. Wong, *Macromol. Rapid Commun.* **2011**, *32*, 1472.
[41] B. J. Littler, M. A. Miller, C. H. Hung, R. W. Wagner, D. F. O'Shea, P. D. Boyle, J. S. Lindsey, *J. Org. Chem.* **1999**, *64*, 1391.
[42] B. Koszarna, D. T. Gryko, *J. Org. Chem.* **2006**, *71*, 3707.
[43] K. E. Thomas, A. B. Alemayehu, J. Conradie, C. Beavers, A. Ghosh, *Inorg. Chem.* **2011**, *50*, 12844.
[44] E. Rabinovich, I. Goldberg, Z. Gross, *Chem. Eur. J.* **2011**, *17*, 12294.
[45] A. Ghosh, T. Wondimagegn, A. B. J. Parusel, *J. Am. Chem. Soc.* **2000**, *122*, 5100.
[46] J. H. Palmer, A. C. Durrell, Z. Gross, J. R. Winkler, H. B. Gray, *J. Am. Chem. Soc.* **2010**, *132*, 9230.
[47] W. Shao, H. Wang, S. He, L. Shi, K. Peng, Y. Lin, L. Zhang, L. Ji, H. Liu, *J. Phys. Chem. B* **2012**, *116*, 14228.
[48] P. Peumans, S. Uchida, S. R. Forrest, *Nature* **2003**, *425*, 158.
[49] M. A. Baldo, C. Adachi, S. R. Forrest, *Phys. Rev. B.* **2000**, *62*, 10967.
[50] Z. Wang, D. Yokoyama, X. F. Wang, Z. Hong, Y. Yang, J. Kido, *Energy Environ. Sci.* **2013**, *6*, 249.
[51] M. Y. Chan, S. L. Lai, M. K. Fung, C. S. Lee, S. T. Lee, *Appl. Phys. Lett.* **2007**, *90*, 023504.
[52] M. Zhang, H. Wang, H. Tian, Y. Geng, C. W. Tang, *Adv. Mater.* **2011**, *23*, 4960.
[53] Y. Liang, Z. Xu, J. Xia, S. T. Tsai, Y. Wu, G. Li, C. Ray, L. Yu, *Adv. Mater.* **2010**, *22*, E135.
[54] T. Ameri, P. Khoram, J. Min, C. J. Brabec, *Adv. Mater.* **2013**, *25*, 4245.
[55] H. Zhou, Y. Zhang, J. Seifter, S. D. Collins, C. Luo, G. C. Bazan, T. Q. Nguyen, A. J. Heeger, *Adv. Mater.* **2013**, *25*, 1646.
[56] Z. Xu, B. Hu, J. Howe, *J. Appl. Phys.* **2008**, *103*, 043909.
[57] A. K. Bansal, W. Holzer, A. Penzkofer, T. Tsuboi, *Chem. Phys.* **2006**, *330*, 118.
[58] W. S. Huang, J. T. Lin, C. H. Chien, Y. T. Tao, S. S. Sun, Y. S. Wen, *Chem. Mater.* **2004**, *16*, 2480.
[59] W. Holzer, A. Penzkofer, T. Tsuboi, *Chem. Phys.* **2005**, *308*, 93.
[60] J. E. Del Bene, W. B. Person, K. Szczepaniak, *J. Phys. Chem.* **1995**, *99*, 10705.
[61] P. J. Hay, W. R. Wadt, *J. Chem. Phys.* **1985**, *82*, 299.
[62] A. D. Becke, *J. Chem. Phys.* **1993**, *98*, 5648.
[63] C. Lee, W. Yang, R. G. Parr, *Phys. Rev. B* **1988**, *37*, 785.
[64] S. H. Vosko, L. Wilk, M. Nusair, *Can. J. Phys.* **1980**, *58*, 1200.
[65] P. J. Stephens, F. J. Devlin, C. F. Chabalowski, M. J. Frisch, *J. Phys. Chem.* **1994**, *98*, 11623.
[66] Y. Zhao, D. G. Truhlar, *Theor. Chem. Acc.* **2008**, *120*, 215.
[67] Y. Zhao, D. G. Truhlar, *J. Chem. Phys.* **2006**, *125*, 194101.
[68] M. Ernzerhof, J. P. Perdew, *J. Chem. Phys.* **1998**, *109*, 3313.
[69] A. D. Boese, N. C. Handy, *J. Chem. Phys.* **2002**, *116*, 9559.
[70] J. Tao, J. P. Perdew, V. N. Staroverov, G. E. Scuseria, *Phys. Rev. Lett.* **2003**, *91*, 146401.
[71] J. Tomasi, B. Mennucci, R. Cammi, *Chem. Rev.* **2005**, *105*, 2999.
[72] M. Cossi, N. Rega, G. Scalmani, V. Barone, *J. Comput. Chem.* **2003**, *24*, 669.
[73] M. F. Lo, T. W. Ng, S. L. Lai, F. L. Wong, M. K. Fung, S. T. Lee, C. S. Lee, *Appl. Phys. Lett.* **2010**, *97*, 143304.
[74] M. Y. Chan, C. S. Lee, S. L. Lai, M. K. Fung, F. L. Wong, H. Y. Sun, K. M. Lau, S. T. Lee, *J. Appl. Phys.* **2006**, *100*, 094506.
[75] M. Y. Chan, S. L. Lai, K. M. Lau, C. S. Lee, S. T. Lee, *Appl. Phys. Lett.* **2006**, *89*, 163515.